

Toward First-Principle Simulations of Galaxy Formation: II. Shock-Induced Starburst at a Collision Interface During the First Encounter of Interacting Galaxies

Takayuki R. SAITOH¹, Hiroshi DAISAKA², Eiichiro KOKUBO^{1,3}, Junichiro MAKINO^{1,3}, Takashi OKAMOTO^{4,5},
Kohji TOMISAKA^{1,3}, Keiichi WADA^{1,3}, Naoki YOSHIDA⁶ (Project Milkyway)

¹ *Center for Computational Astrophysics, National Astronomical Observatory of Japan, 2-21-1 Osawa, Mitaka-shi, Tokyo 181-8588*

² *Graduate School of Commerce and Management, Hitotsubashi University, Naka 2-1 Kunitachi-shi, Tokyo 186-8601*

³ *Division of Theoretical Astronomy, National Astronomical Observatory of Japan, 2-21-1 Osawa, Mitaka-shi, Tokyo 181-8588; and School of Physical Sciences, Graduate University of Advanced Study (SOKENDAI)*

⁴ *Institute for Computational Cosmology, Department of Physics, Durham University, South Road, Durham, DH1 3LE, UK*

⁵ *Center for Computational Sciences, University of Tsukuba 1-1-1, Tennodai, Tsukuba, Ibaraki 305-8577, Japan*

⁶ *Institute for the Physics and Mathematics of the Universe, University of Tokyo, 5-1-5 Kashiwanoha, Kashiwa, Chiba 277-8568, Japan*

saitoh.takayuki@nao.ac.jp, saitoh.takayuki@cfca.jp

(Received 2008 April 28; accepted 2009 January 7)

Abstract

We investigated the evolution of interacting disk galaxies using high-resolution N -body/SPH simulations, taking into account the multiphase nature of the interstellar medium (ISM). In our high-resolution simulations, a large-scale starburst occurred naturally at the collision interface between two gas disks at the first encounter, resulting in the formation of star clusters. This is consistent with observations of interacting galaxies. The probability distribution function (PDF) of gas density showed clear change during the galaxy-galaxy encounter. The compression of gas at the collision interface between the gas disks first appears as an excess at $n_{\text{H}} \sim 10 \text{ cm}^{-3}$ in the PDF, and then the excess moves to higher densities ($n_{\text{H}} \gtrsim 100 \text{ cm}^{-3}$) in a few times 10^7 years where starburst takes place. After the starburst, the PDF goes back to the quasi-steady state. These results give a simple picture of starburst phenomena in galaxy-galaxy encounters.

Key words: galaxies:starburst — galaxies:ISM — ISM:structure — method:numerical

1. Introduction

Galaxy-galaxy interactions (collisions and mergers) are believed to play important roles in shaping present-day galaxies, since they occur frequently in the standard hierarchical model of galaxy formation (e.g., White & Rees 1978; Lacey & Cole 1993; Kauffmann & Charlot 1998; Okamoto & Nagashima 2001). Interactions drive not only morphological transformations of galaxies but also bursts of star formation (e.g., Young et al. 1986; Barnes & Hernquist 1992; Smith et al. 2007; Li et al. 2008).

A number of researchers have studied roles of galaxy-galaxy interactions using numerical simulations (e.g., Toomre & Toomre 1972; Hernquist 1989; Mihos & Hernquist 1994; Mihos & Hernquist 1996; Barnes & Hernquist 1996; Springel 2000; Cox et al. 2004; Springel & Hernquist 2005; Cox et al. 2006). Many simulations incorporated the interstellar medium (ISM) and models for star formation and supernova (SN) feedback from massive stars. In such simulations, the numerical resolution is rather limited. The typical gas mass resolution is about $10^6 M_{\odot}$. Because of this limited mass resolution, it was impossible to treat the formation of cold gas phase be-

low 10^4 K . (see §2 in Saitoh et al. 2008; hereafter paper I). In most of early simulations, an isothermal equation of state (EOS) of 10^4 K was used for the ISM (e.g., Mihos & Hernquist 1996). Even when the energy equation with a cooling term was used, the minimum temperature was set to be $\sim 10^4 \text{ K}$ (e.g., Barnes & Hernquist 1996). Some authors (Springel 2000; Cox et al. 2004) adopted the EOS that became harder in higher density. They argued that such EOS mimicked the effect of turbulence motions caused by SNe feedback from massive stars. Struck (1997) employed a multiphase ISM model involving a low-temperature phase under 10^4 K , although the modeling of ISM was rather simple and mass resolution was low.

Low-resolution simulations did not work well under the situation of strong galaxy-galaxy interactions. Observations of interacting galaxies often show shock-induced, widespread star-formation activities involving star cluster formation (e.g., the Antennae and the Mice galaxies), whereas previous simulations showed that most of star formation activities was concentrated to the central regions of the galaxies. Barnes (2004) demonstrated that the collision simulations with the isothermal ISM and the star-formation model governed by the local energy dissi-

pation rate in shocks can reproduce large-scale starburst formed at the collision interface during the first collision. However, his shock-induced star formation model introduced an additional parameter and required the fine tuning of model parameters for star formation.

The Schmidt law (Schmidt 1959) has been used as star formation model;

$$\frac{d\rho_*}{dt} = C_* \frac{\rho_{\text{gas}}}{t_{\text{dyn}}}, \quad (1)$$

where ρ_* and ρ_{gas} are the stellar density and gas density, respectively, $t_{\text{dyn}} = (4\pi G \rho_{\text{gas}})^{-1/2}$ is the local dynamical time, and C_* is the dimensionless star formation efficiency. Since the isothermal EOS prevents ISM to form small-scale structures, in most simulations, stars had to be formed in fairly low-density gas. Recent models employ the threshold density for star formation, $n_{\text{H}} \sim 0.1 \text{ cm}^{-3}$, above which star formation occurs. SNe releases energy into the surrounding ISM in the form of thermal or kinetic energy, or internal turbulence motions. When the value of C_* was appropriately tuned, simulations based on these models successfully reproduced observed global properties of star formation in local disk galaxies, in particular the Schmidt-Kennicutt relation (Kennicutt 1998). However, simulations with the isothermal EOS or the temperature cutoff in cooling functions at 10^4 K failed to reproduce three-dimensional structure of star formation activities, simply because the star formation in these simulation took place effectively everywhere in the gas disk. In paper I, we demonstrated that high-resolution simulation of the ISM with low temperature cooling below 10^4 K , combined with higher threshold density for star formation, gave rise to thin and inhomogeneous star forming regions as observed in isolated disk galaxies. Our high-resolution simulations gave a good description of small-scale structures of star forming regions, and at the same time well reproduced global characteristics such as the Schmidt-Kennicutt relation.

In this paper, we report the results of high-resolution simulations of a collision between two disk galaxies with realistic ISM with cooling term and high-density star-formation criterion for the Schmidt-type star formation model. This ISM model is based on the one used in paper I and it can reproduce properties of star-formation in local disk galaxies, without the fine tuning of the value of C_* . Our main conclusion is that high-resolution simulations can resolve shock-compressed regions, and, as a result, these simulations can naturally reproduce a large-scale starburst at the collision interface of gas disks during the first encounter. Initially, the density of the gas in the shock-compressed region reaches $n_{\text{H}} \sim 10 \text{ cm}^{-3}$. This compressed gas collapses through radiative cooling and gravitational instability in the timescale of $\sim 10^7 \text{ yr}$ and reaches a high density at which star formation is triggered. Thus, our modeling of the ISM, which requires sufficiently high-resolution, naturally reproduces the shock-induced starburst. A comparison run, which was performed with the temperature cutoff in cooling function at 10^4 K and relatively low-density threshold for star-formation, displays

only a small enhancement of the star formation rate (SFR) during the first encounter. By using high-resolution simulations with a realistic star formation model, we can successfully reproduce not only the quiescent star formation in disk galaxies (paper I) but also the large-scale starburst at a collision interface and nuclear starbursts observed in interacting galaxies without any extra assumptions.

2. Method and setup

We used a parallel tree SPH code ASURA (Saitoh, in preparation) that utilizes the special-purpose hardware GRAPE. We first constructed near-equilibrium, self-consistent galaxy models with a dark-matter halo and an exponential disk, and then we converted a part of particles into gas particles. The N -body realization was generated by GalactICS (Kuijken & Dubinski 1995). Our galaxy model is a low-mass, gas rich Sc galaxy with the characteristic rotation velocity of 120 km s^{-1} . It has a gradually increasing rotation curve, which is consistent with observations of nearby low-mass galaxies (Sofue et al. 1999). The dark-matter halo mass and the disk mass are $1.05 \times 10^{11} M_{\odot}$ and $6.3 \times 10^9 M_{\odot}$, respectively. The scale length of the exponential disk is set to be 4 kpc (Roberts & Haynes 1994). We converted 20 % of the disk particles, $1.2 \times 10^9 M_{\odot}$, into gas particles with the exponential profile of an 8 kpc scale length. We also converted 1 % of the dark matter particles into gas particles with the same profile as that of the dark matter halo. The initial gas temperature is set to be 10^4 K . The galaxy-galaxy collision is characterized by a prograde parabolic orbit with the pericentric distance $R_{\text{peri}} = 7.5 \text{ kpc}$ and the initial separation of 75 kpc. The relative velocity at the moment of the pericenter passage is $\sim 370 \text{ km s}^{-1}$ for the point-mass approximation. Two galaxies have the same spin direction. We prepare three initial models with different mass resolutions. Further details of the set up are described in Saitoh et al. (in preparation). The gravitational softening was set to be 20 pc for all particles in all runs. The particle mass and number of particles are summarized in table 1.

We use a cooling function for a gas with the metallicity of half the solar value for the temperature range from 10 K to 10^8 K (Spaans & Norman 1997; Wada & Norman 2001). A uniform heating from the far-ultraviolet radiation is included. The intensity of the far-ultraviolet radiation is set to be the half of the solar neighborhood value (Wolfire et al. 1995).

Models for the star formation and the SNe feedback are similar to those in paper I. We first adopt the model which allows a wide range of temperature for ISM ($10 - 10^8 \text{ K}$) and uses the values 100 cm^{-3} and 100 K as the threshold density and temperature for the star-formation, respectively. We add the label ‘C’ in run names for these models. For comparison, we perform a run which only allows the ISM temperature above 10^4 K and employs 0.1 cm^{-3} and 15000 K as the threshold density and temperature for the star-formation, respectively. The behavior of the ISM in this run should be similar to those in previous simulations

with isothermal ISM of $\sim 10^4$ K. The label ‘A’ indicates this model. We adopt $C_* = 0.033$ for all runs.

3. Starburst during the first encounter

Figure 1 shows global SFR during the first encounter. Before the encounter, each galaxy has a nearly constant SFR of $\sim 1 M_\odot \text{ yr}^{-1}$. For Runs M1C, M2C, and M3C, SFR increases by almost an order of magnitude just after the pericenter passage (~ 430 Myr; see the thin curve). We call this peak as a *starburst*. This duration of the starburst is short and the phase of star formation returns quickly to the quiescent star-formation phase after the first passage. The slightly larger SFR than those seen in the pre-collision might be explained by strong non-axisymmetric perturbations from the companion galaxy (Noguchi 1988). The behavior of the starburst at the first encounter is similar to that obtained by Barnes (2004) who implemented a shock-induced star formation. Also, the difference between Runs M1C, M2C, and M3C is very small. We conclude that our result is independent of the mass resolution as long as the resolution is sufficiently high. In contrast to these ‘C’ runs, Run M1A shows very small enhancement of SFR during the first encounter.

The difference in SFR is owing to the hydrodynamic pressure of the gas that forms a bulk of the giant filament. The pressure of gas in Run M1A is roughly a thousand times larger than those in Runs M1C, M2C, and M3C at the same density, because the gas in Run M1A can not cool below 10^4 K while those in Runs M1C, M2C, and M3C can cool down to 10 K. In Run M1A, the high pressure ISM in the contact interface resists collapse even under significant compression. As a result, the density of the ISM is not increased significantly at the interface. Since the timescale of the pericenter passage of the galaxy-galaxy interaction is not very long (say, 10^7 years), in Run M1A, a smaller amount of the stars are formed during the first encounter, as long as we adopt the Schmidt law for the modeling of the star formation.

Figure 2 shows the gas density of Run M2C at the orbital plane for six different epochs. Two galaxies first follow the parabolic orbit and then collide at the pericenter (top panels). During the first encounter, the maximum Mach number reaches ~ 100 for the cold ($T < 100$ K) gas. The ISM at the collision interface is strongly compressed by shocks and forms a large and dense filament (see the top-right panel of figure 2; $t = 420$ Myr). We call it a *giant filament*. The length of this giant filament at its formation epoch is ~ 10 kpc. We measured the gas mass in the rectangular box of the size $10 \text{ kpc} \times 2 \text{ kpc} \times 2 \text{ kpc}$ along the giant filament (the black rectangular box in the top-right panel of figure 2). The gas mass of the giant filament is $\sim 9 \times 10^8 M_\odot$. This mass is about one quarter of the total gas mass in the system. The stellar mass formed during the starburst phase ($t = 420 - 450$ Myr) becomes ~ 20 % of the initial filament mass. The distribution of star forming regions is consistent with observations in interacting galaxies (e.g., Whitmore & Schweizer 1995). Overall evolution of the colliding galaxies in the first encounter is

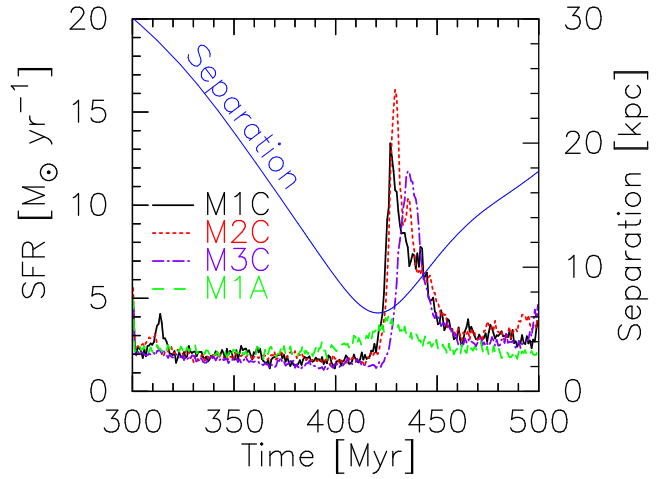


Fig. 1. Global SFR during the first encounter as a function of time. Thick solid, dotted, dot-dashed, and dashed curves indicate the global SFR for Runs M1C, M2C, M3C, and M1A, respectively. The thin curve indicates the separation between two galactic centers.

quite different from those in previous simulations with the isothermal ISM and the Schmidt-type star formation models. Our high-resolution simulation naturally captures the shock-induced, large-scale starburst at the collision interface. A number of “star clusters” form in the giant filament at the starburst phase. We will study the formation of the star clusters in further details in forthcoming papers.

In addition to the shock-induced starburst in the giant filament, we also find the starburst during a core-merging phase. Figure 3 follows the evolution of SFR during this phase. As is shown in this figure, simulations with our model shows starbursts with multiple peaks in the final core-merge phase. The star formation mainly takes place within compact clumps in this phase. This is consistent with the observations of ULIRGs (Sanders & Mirabel 1996). Our simulations successfully reproduce the nuclear starbursts as well as the large-scale starbursts. We further find the star formation enhancement in the tidal tails.

4. Probability distribution function during the starburst

Figure 4 shows the volume weighted probability distribution function (PDF) of Run M2C for several different epochs before, during, and after the first encounter. Although there are some noticeable changes in the PDF with time, they are difficult to see because of the large vertical scale. In order to see the changes in the density distribution of the gas more clearly, we plot the mass functions of the gas, $dM/d\log(n_H)$, in figure 5. Just before the encounter ($t = 410$ Myr), an excess of the gas (bump) appears at $n_H \sim 10 \text{ cm}^{-3}$. By $t = 430$ Myr, this bump moved to $n_H \gtrsim 100 \text{ cm}^{-3}$, and by $t = 450$ Myr it almost vanished. Note that this period of $t = 430 - 450$ Myr coincides with the period of the starburst. Thus, we

Table 1. Number and mass of particles for initial conditions of merger simulations. The cutoff temperature for the ISM, threshold density and temperature and efficiency for star formation are also listed.

Run	N_{DM}^{a}	$N_{\text{Disk}}^{\text{b}}$	$N_{\text{Gas}}^{\text{c}}$	m^{d}	$T_{\text{cut}}^{\text{e}}$	n_{th}^{f}	T_{th}^{g}	C_*^{h}
M1A	6 930 000	341 896	148 104	$3 \times 10^4 M_{\odot}$	10^4 K	0.1 cm^{-3}	15000 K	0.033
M1C	6 930 000	341 896	148 104	$3 \times 10^4 M_{\odot}$	10 K	100 cm^{-3}	100 K	0.033
M2C	13 860 000	683 678	296 322	$1.5 \times 10^4 M_{\odot}$	10 K	100 cm^{-3}	100 K	0.033
M3C	27 720 000	1 361 012	598 988	$7.6 \times 10^3 M_{\odot}$	10 K	100 cm^{-3}	100 K	0.033

^aThe number of DM particles. ^bThe number of disk particles. ^cThe initial number of SPH particles. ^dMass of individual particles (M_{\odot}). ^eCutoff temperature of cooling function (K). ^fThreshold density of star formation (cm^{-3}). ^gThreshold temperature of star formation (K). ^hStar formation efficiency.

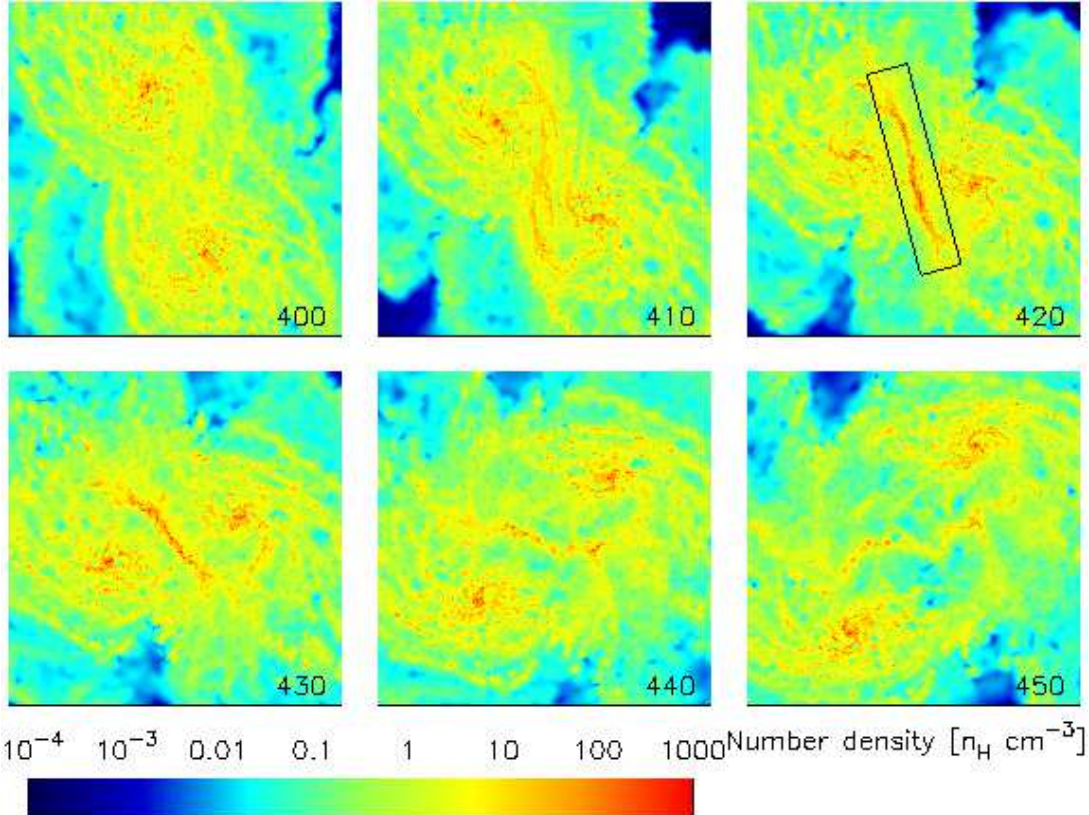


Fig. 2. Gas density distribution for Run M2C. Each panel shows a $16 \text{ kpc} \times 16 \text{ kpc}$ region. The elapsed time in Myr is shown the right-bottom corner of each panel.

have a simple and clear picture of the shock-induced starburst; Initially, large amounts of the gas is compressed to $n_{\text{H}} \sim 10 \text{ cm}^{-3}$. Then, this compressed gas cools and become denser through gravitational instability, and when the gas becomes dense enough to form stars, the starburst takes place. The starburst is led mainly by star formation in massive clusters. After the high-density gas is consumed, the density PDF returns to the quasi-steady state. In figure 6, we show the time variation of the mass in selected density ranges. The relative changes are larger for higher densities. Moreover, the peak is found at systematically later epochs for higher densities. The time delay from $n_{\text{H}} = 10 \text{ cm}^{-3}$ to 100 cm^{-3} is 10 Myr. This timescale corresponds to the local dynamical time, $t_{\text{dyn}}(n_{\text{H}} = 10 \text{ cm}^{-3}) \sim 10 \text{ Myr}$, and it is

faster than the mean evolution timescale in isolated disk galaxies ($\sim 5 t_{\text{dyn}}$; see figure 10 in paper I). The lifetime of the mass excess in each density range in figure 6 is around 20 Myr. As is expected, this timescale corresponds to that of the starburst.

5. Summary

We have studied the evolution of the multiphase ISM in the colliding galaxies. Our simulations, for the first time, resolved the shock-induced gas compression and starburst at the collision interface during the first encounter of colliding galaxies, with the density dependent star formation model (the Schmidt law). The behavior of the ISM is qualitatively different from the results of previous studies

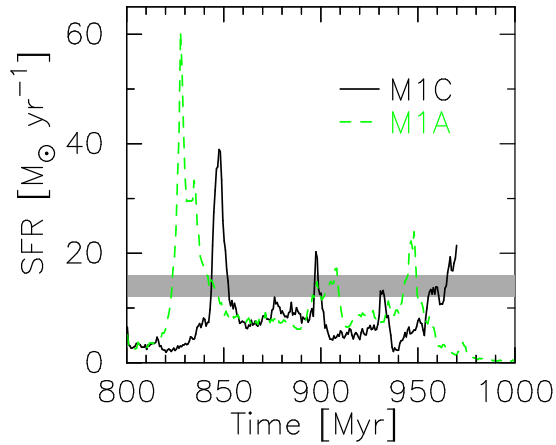


Fig. 3. Global SFR during the core-merger phase as a function of time. Thick solid and dotted curves indicate the global SFR for Runs M1C and M1A, respectively. For reference, the peak SFRs at the first encounter is $12 - 16 M_{\odot} \text{ yr}^{-1}$ (the horizontal gray zone), which is small to the SFR peaks in the core-merger phase shown here.

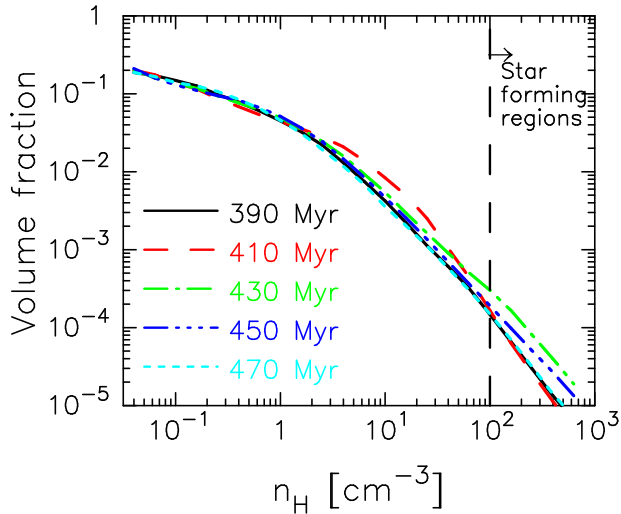


Fig. 4. Volume weighted probability distribution functions for the gas of Run M2C for five different epochs. The gas within $R < 10 \text{ kpc}$ and $|Z| < 1 \text{ kpc}$, where R is the distance from the mid-point of two galaxies at the initial time in the orbital plane and Z is the vertical height from the orbital plane, is considered.

with isothermal ISM.

Shock-induced starbursts, which have been observed in many interacting galaxies, naturally take place in our high-resolution simulations without any extra assumptions for the star-formation, such as the dependence on the energy dissipation rate (Barnes 2004; Okamoto et al. 2005). In previous simulations with limited resolutions, significant shock-induced starbursts took place only when the presence of the shock itself is used as the criterion for star formation.

In paper I, we showed that high-resolution simulations with realistic ISM and high-density star-formation criterion can reproduce the Schmidt-Kennicutt relation with-

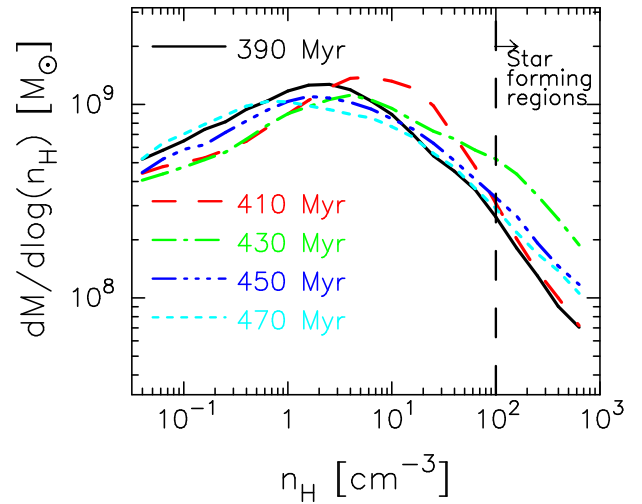


Fig. 5. Mass distribution as a function of the density of Run M2C for five different epochs. All gas in the system is included.

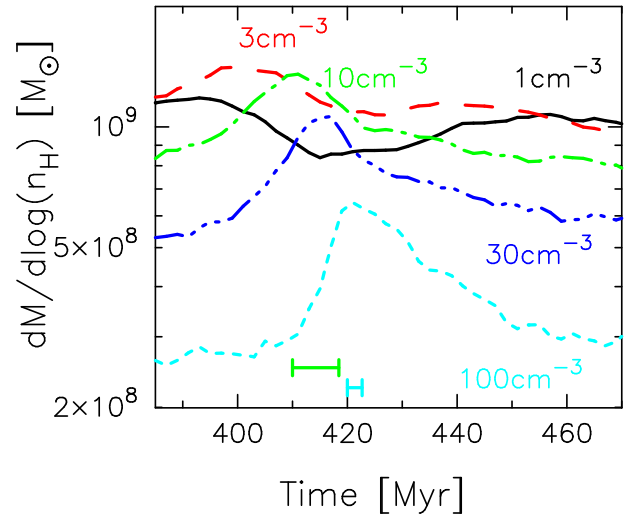


Fig. 6. Time evolution of gas mass for five different density ranges. Long (green) and short (light blue) horizontal bars correspond to local dynamical times of densities at $n_H = 10 \text{ cm}^{-3}$ and 100 cm^{-3} , respectively.

out the need of the fine tuning of the value of C_* . Previous simulations with isothermal ISM and low-density star-formation criterion required fine tuning. In this paper, we showed that high-resolution simulations can directly resolve shock-compressed regions and these simulations can automatically reproduce shock-induced starbursts. High-resolution (particle mass less than $10^4 M_{\odot}$) with a realistic star formation model allows us to study both quiescent star formation and starburst modes in N -body/SPH simulations of galaxy formation.

We thank the anonymous referee for his/her insightful comments and suggestions, which helped us to greatly improve our manuscript. The author (TRS) thanks Sachiko Onodera and Shinya Komugi for helpful dis-

cussions. Numerical computations were carried out on Cray XT4/GRAPE system (project ID:g07a19/g08a19) at CfCA of NAOJ. This project is supported by Grant-in-Aids for Scientific Research (17340059) of JSPS and Molecular-Based New Computational Science Program of NINS.

References

- Barnes, J. E. 2004, *MNRAS*, 350, 798
 Barnes, J. E., & Hernquist, L. 1992, *ARA&A*, 30, 705
 —. 1996, *ApJ*, 471, 115
 Cox, T. J., Jonsson, P., Primack, J. R., & Somerville, R. S. 2006, *MNRAS*, 373, 1013
 Cox, T. J., Primack, J., Jonsson, P., & Somerville, R. S. 2004, *ApJL*, 607, L87
 Hernquist, L. 1989, *Nature*, 340, 687
 Kauffmann, G., & Charlot, S. 1998, *MNRAS*, 294, 705
 Kennicutt, Jr., R. C. 1998, *ApJ*, 498, 541
 Kuijken, K., & Dubinski, J. 1995, *MNRAS*, 277, 1341
 Lacey, C., & Cole, S. 1993, *MNRAS*, 262, 627
 Li, C., Kauffmann, G., Heckman, T. M., Jing, Y. P., & White, S. D. M. 2008, *MNRAS*, 385, 1903
 Mihos, J. C., & Hernquist, L. 1994, *ApJ*, 437, 611
 —. 1996, *ApJ*, 464, 641
 Noguchi, M. 1988, *A&A*, 203, 259
 Okamoto, T., Eke, V. R., Frenk, C. S., & Jenkins, A. 2005, *MNRAS*, 363, 1299
 Okamoto, T., & Nagashima, M. 2001, *ApJ*, 547, 109
 Roberts, M. S., & Haynes, M. P. 1994, *ARA&A*, 32, 115
 Saitoh, T. R., Daisaka, H., Kokubo, E., Makino, J., Okamoto, T., Tomisaka, K., Wada, K., & Yoshida, N. 2008, *PASJ*, 60, 667
 Sanders, D. B., & Mirabel, I. F. 1996, *ARA&A*, 34, 749
 Schmidt, M. 1959, *ApJ*, 129, 243
 Smith, B. J., Struck, C., Hancock, M., Appleton, P. N., Charmandaris, V., & Reach, W. T. 2007, *AJ*, 133, 791
 Sofue, Y., Tutui, Y., Honma, M., Tomita, A., Takamiya, T., Koda, J., & Takeda, Y. 1999, *ApJ*, 523, 136
 Spaans, M., & Norman, C. A. 1997, *ApJ*, 483, 87
 Springel, V. 2000, *MNRAS*, 312, 859
 Springel, V., & Hernquist, L. 2005, *ApJL*, 622, L9
 Struck, C. 1997, *ApJS*, 113, 269
 Toomre, A., & Toomre, J. 1972, *ApJ*, 178, 623
 Wada, K., & Norman, C. A. 2001, *ApJ*, 547, 172
 White, S. D. M., & Rees, M. J. 1978, *MNRAS*, 183, 341
 Whitmore, B. C., & Schweizer, F. 1995, *AJ*, 109, 960
 Wolfire, M. G., Hollenbach, D., McKee, C. F., Tielens, A. G. G. M., & Bakes, E. L. O. 1995, *ApJ*, 443, 152
 Young, J. S., Kenney, J. D., Tacconi, L., Claussen, M. J., Huang, Y.-L., Tacconi-Garman, L., Xie, S., & Schloerb, F. P. 1986, *ApJL*, 311, L17